Check for updates

Light-driven folding of single polymer chains *via* metal-complexation†

Aidan E. Izuagbe,[a,b] Bryan T. Tuten, [ID] *[a] Peter W. Roesky [ID] *[b] and Christopher Barner-Kowollik [ID] *[a,c]

We introduce a light-driven methodology (λ_{max} = 365 nm) to fold single polymer chains into single chain nanoparticles (SCNPs). Exploiting the photo-isomerization of spiropyran entities embedded into the backbone of polymer chains (ranging from 15 to 38 mol%) constituted of polyethylene glycol carrying monomer units (ranging from M_n = 28 500 g mol^{-1} to 40 000 g mol^{-1}), we complex their open form using a range of metals, including iron, copper and cobalt. The approach offers the first direct avenue for incorporating metals into SCNPs *via* a photochemical folding mechanism in one step.

Introduction

Single chain polymer nanoparticles (SCNPs) have in recent years evolved from macromolecular architectural curiosities to functional soft matter materials that are exploited as *e.g.* catalysts, combining the advantages of homogeneous and heterogeneous catalysis as well as sensors.[1–3] While the field explores both the physical and chemical properties to elucidate their folding behaviour and physical properties,[4–7] current work is focused on harnessing the utility of precision folded systems in conjunction with advanced chemical modification of the intramolecular crosslinks and backbone to generate entities capable of specific catalysis.[8–10] Indeed, perhaps the fastest growing field within functional SCNPs is in the realm of catalytic materials.[11–13] Due to the formation of hydrophilic and hydrophobic pockets, drastically increased surface area, and a high functional density, SCNP catalytic systems have demonstrated promise across various chemical systems.[14–16] A particular challenge with functional organometallic systems is the requirement for a specific ligand design dependent on the targeted metal centre. Thus, ideally, the ligand system should be agnostic to a wide array of metal centres, which is critically lacking in the current SCNP design toolbox. Further, the

folding of the parent polymer chains into SCNPs should ideally proceed at ambient temperature under the mildest possible conditions. Photons are considered a traceless reagent and especially long visible light wavelengths are ideally suited to induce chemical transformation in a very mild fashion. In the current contribution, we introduce an avenue to install metal centres into SCNPs *via* a light-driven photochemical process exploiting the switching of spiropyrans into their ring-opened form, which can in the open state effectively react with metal ions to form a stable complex (refer to Scheme 1).

Results and discussion

Spiropyrans are versatile photoswitches, which have received increasing attention over the years and are highly attractive entities in their ring-opened merocyanine form for follow-on chemistry by virtue of the generated negatively charged oxygen atom that can, for example, serve as a coordinating ligand.[17–19] Herein, we incorporate several metal centers into SCNPs without the use of an additional crosslinker in a simple one step reaction using photons. We base our polymer on a backbone of a methyl methacrylate carrying poly(ethylene glycol) side chains (PEGMEMA), and a methacrylate functionalised spiropyran (refer to the ESI section 2† for characterization and synthetic methods detailing the polymer and small molecule synthesis) allowing for optimal solubility in a mixture of methanol and dioxane. We prepare three polymers (M_n = 28 500, 30 500 and 40 000 g mol^{-1}) with different ratios of the copolymerized spiropyran-functional monomer (refer to Table 1 for the SEC characterisation data).[20,21] Fig. 1 displays the ^{1}H-NMR spectrum of the 36 mol% containing polymer (**SP-36-PEGMEMA**) from which the exact polymer composition

[a]School of Chemistry and Physics, Centre for Materials Science, Queensland University of Technology (QUT), 2 George Street, Brisbane, Queensland 4000, Australia. E-mail: christopher.barnerkowollik@qut.edu.au, bryan.tuten@qut.edu.au
[b]Institute of Inorganic Chemistry, Karlsruhe Institute of Technology (KIT), Engesserstr. 15, 76131 Karlsruhe, Germany. E-mail: peter.roesky@kit.edu
[c]Institute of Nanotechnology (INT), Karlsruhe Institute of Technology (KIT), Hermann-von-Helmholtz-Platz 1, 76344 Eggenstein-Leopoldshafe, Germany. E-mail: christopher.barner-kowollik@kit.edu

†Electronic supplementary information (ESI) available: Synthetic methodologies, compound spectral information, emission and absorption spectra, methods and instrumentation. See DOI: https://doi.org/10.1039/d4py00280f
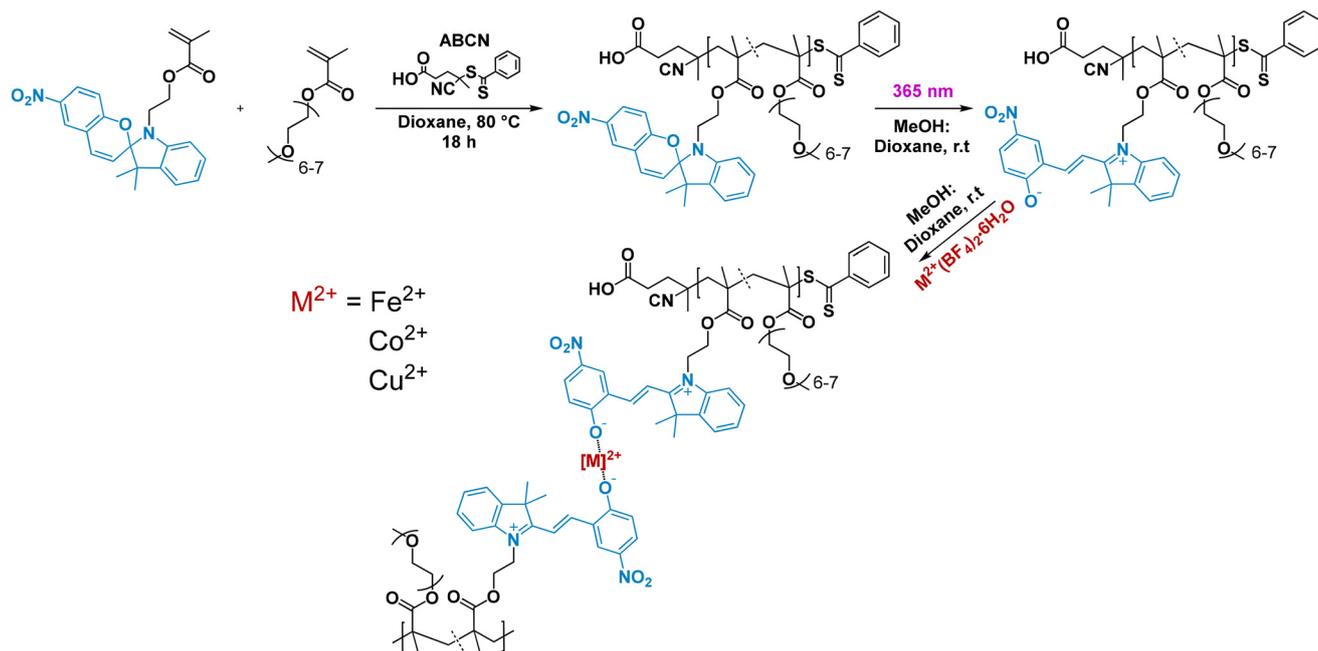
Scheme 1 Overview of the SCNP design strategy followed in the current contribution based on a methyl methacrylate with poly(ethylene glycol) side chains and photoreactive spiropyran (SP) units (**SP-X-PEGMEMA**) with different compositions, where X is the mol% of spiropyran units. The spiropyran metal coordination sphere [M²⁺] is likely completed by solvent molecules and shown here in a simplified way. Note that the crosslinking occurs within one polymer chain intramolecularly.

Table 1 Dispersity and molecular weights of the SP-X-PEGMEMA polymers reported as both number average and peak molecular weights, derived from SEC measurements in THF using PMMA calibration standards

	M_p/g mol⁻¹	M_n/g mol⁻¹	Đ
SP-15-PEGMEMA	32 000	30 500	1.3
SP-36-PEGMEMA	45 000	40 000	1.2
SP-38-PEGMEMA	29 500	28 500	1.4

has been deduced as well as its corresponding SEC (THF) chromatogram. The corresponding analytical data for the 15 and 38 mol% spiropyran containing polymers can be found in the ESI sections 2 and 4.3.†

Due to the propensity of spiropyran to undergo significant photo degradation upon conversion to the merocyanine isomer, it is critical to establish an understanding of the photoswitching properties of the employed spiropyran system.[17,22] The photoswitching characteristics were thus investigated on one of the linear, spiropyran decorated polymers, *i.e.* **SP-36-PEGMEMA**, to identify irradiation conditions for the subsequent folding experiments. A solvent mixture of dioxane : methanol 1 : 6 was selected to facilitate efficient photoswitching (methanol) and polymer solubility (dioxane) and used for all subsequent photochemical characterisations. The linear polymer (0.0143 mmol L⁻¹, 0.5 g L⁻¹) was subjected to varying irradiation times with a 7 mW LED centred at 365 nm (refer to the ESI Fig. S21† for the LED's emission spec-

trum). The degree of spiropyran to merocyanine conversion was determined by monitoring the λ_{max} of the visible region at close to 552 nm. Similar absorption at 552 nm was observed for 1, 2 and 3 min of continuous irradiation (Fig. 2A and B).

Periodic irradiation at 365 nm for 1 min and white light irradiation (refer to Fig. S22† for the emission spectrum) for 1 min to generate the merocyanine entities and recovery of the spiropyran respectively was conducted to determine the fatigue resistance of the spiropyran polymer. Photo-induced fatigue was evidenced as a loss in intensity of the visible band centred at 552 nm (Fig. 2C). Consequently, only 1 min irradiation times were employed for the subsequent folding experiments. The band centred at 552 nm was once more used to track the gradual thermal reversion of the merocyanine isomer to the closed spiropyran. As a highly solvent dependent process, increased thermal stability is reported for spiropyran switching in polar solvents.[23] As the charged merocyanine form is responsible for forming intramolecular metal-crosslinks and collapsing the polymer chain, the presence of a thermally stable, long lived merocyanine isomer is critical.[24] Accordingly, when irradiated in the noted methanol/dioxane mixture, the linear spiropyran polymer features a merocyanine isomer with a long thermal half-life, gradually relaxing back near-quantitatively to the closed spiropyran within a 1 h period (Fig. 2D). The photochemical folding of linear spiropyran polymers into SCNPs was conducted in a photo vial with a 7 W LED centred at 365 nm (refer to the ESI Fig. S2† for a photograph of the reaction set-up). A solution of dissolved metal salt in methanol (0.021 mol L⁻¹, 7.05 g L⁻¹) was added
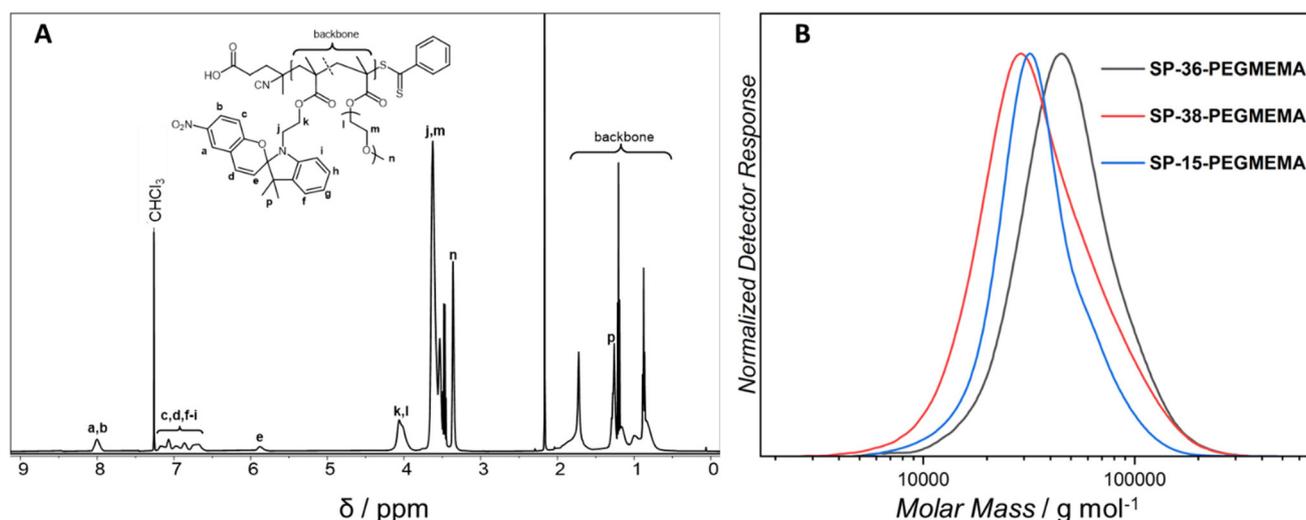
Fig. 1 (A) Exemplary ^{1}H NMR spectrum of **SP-36-PEGMEMA** in deuterated chloroform recorded at 500 MHz. The ^{1}H-NMR spectra of the additional polymers can be found in the ESI (ESI, Fig. S19 and S20†). (B) SEC traces of the parent polymers, **SP-15-PEGMEMA**, **SP-36-PEGMEMA** and **SP-38-PEGMEMA**. The folding is induced by mild UV-light (λ_{max} = 365 nm), ring opening the spiropyran units within the polymer chains, which subsequently react with copper, iron and cobalt ions contained in metal salts.
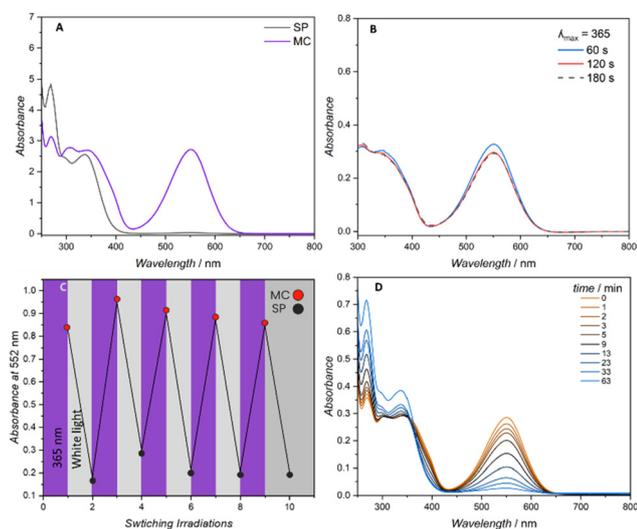

Fig. 2 UV-Vis spectroscopy of **SP-36-PEGMEMA** dissolved in a dioxane/methanol mixture. (A) UV-Vis of **SP-36-PEGMEMA** spectrum after irradiation for 1 min with a 365 nm centred LED affording the open merocyanine (MC) form of the polymeric spiropyran (SP) pendant groups, indicated by an increase in the absorption band centred at 552 nm. (B) Effect of increasing irradiation time on the generation of **SP-36-PEGMEMA** bound spiropyran into merocyanine units. (C) Periodic irradiation of **SP-36-PEGMEMA** with 365 nm and subsequent white light irradiation. The absorption band at 552 nm was used to monitor the formation of the merocyanine and spiropyran isomers. (D) Thermal relaxation in dioxane : methanol 1 : 6 of the merocyanine isomers generated by 365 nm irradiation within **SP-36-PEGMEMA**, monitored over 1 h by UV-Vis spectroscopy.

via a syringe pump *via* continuous addition to a solution of the respective spiropyran polymer in the noted dioxane : methanol 1 : 6 mixture (0.5 mg mL^{-1}), periodically irradiated

with a 365 nm LED. As noted, to avoid photo-induced fatigue, irradiation was limited to 1 min pulses interluded by 30 min of stirring in the dark. The relatively long thermal half-life in dioxane/methanol and the high amount of merocyanine generated after even 1 min irradiation allows for a sufficiently high concentration of merocyanine units for metal ion complexation without continuous irradiation (refer to ESI Fig. S3† for the irradiation pattern and setup). Size exclusion chromatography (SEC) using THF as an eluent was used to monitor the compaction of the linear polymer into SCNPs. A decrease in apparent molecular weight is indictive of intramolecular compaction and SCNP formation.[25] Both the number average molecular weight (M_n) and peak molecular weight (M_p) are commonly used to evidence compaction. The resulting compactions are summarised in Table 2 and the corresponding SEC traces can be found in Fig. 4.

Compaction of **SP-38-PEGMEMA** (38 mol% spiropyran units) was most significant with the introduction of Fe^{II} ions after 365 nm irradiation with a reduction in apparent molecular weight of 25%. Co^{II} and Cu^{II} ions induced SCNP formation, albeit with less compaction for the same polymer. As an independent assessment of the compaction, an exemplary DOSY spectrum (Fig. 3) was recorded for the Fe^{II}-SCNP originating from **SP-38-PEGMEMA**. The derived diffusion coefficients were used to estimate a hydrodynamic diameter of 5.08 nm for the Fe^{II}-SCNP indicating a 16% compaction when compared to the parent polymer **SP-38-PEGMEMA** featuring a diameter close to 6.06 nm (for the primary DOSY data of both the Fe^{II}-SCNP and **SP-38-PEGMEMA** refer to ESI section 6†).

Critically, a control experiment was conducted to ensure that SCNP formation did not occur in the dark or at a slower rate compared with the irradiated samples (refer to the ESI, Fig. S4 and section 3.4† for the procedure). Specifically,

Table 2 Relative compaction (in percent) achieved using the precursor polymers denoted SP-*X* with different molar contents of spiropyran units with varying metal salt precursors. Folding with the 15 mol% polymer was attempted only with Fe(BF$_4$)$_2$ and Co(BF$_4$)$_2$. Refer to the ESI section 3.1† for the exact compaction procedure for each metal salt. Note that the reported molecular weights are apparent

	Co(BF$_4$)$_2$			Fe(BF$_4$)$_2$		
	M_p/g mol^{-1}	M_n/g mol^{-1}	% comp	M_p/g mol^{-1}	M_n/g mol^{-1}	% comp
SP-15	31 500	31 500	2	30 000	30 500	6
SP-36	36 000	32 500	20	n/a	n/a	n/a
SP-38	26 000	21 000	12	22 000	14 000	25

	Ni(BF$_4$)$_2$			Zn(BF$_4$)$_2$		
	M_p/g mol^{-1}	M_n/g mol^{-1}	% comp	M_p/g mol^{-1}	M_n/g mol^{-1}	% comp
SP-36	43 000	39 000	4	42 000	39 500	7

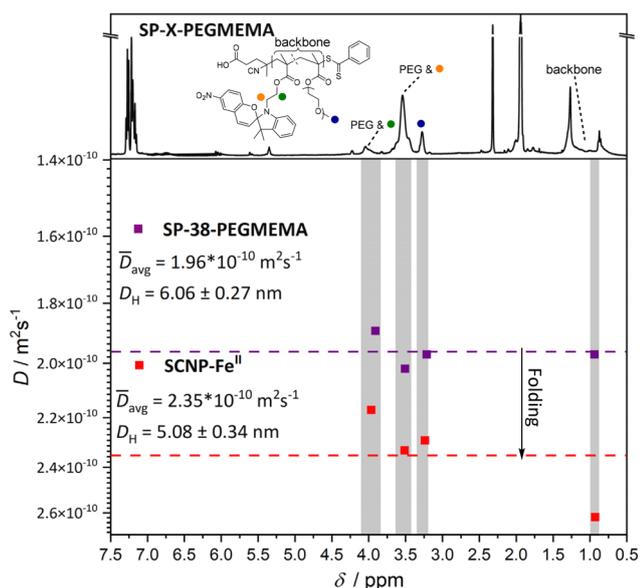|	Cu(BF$_4$)$_2$		
	M_p/g mol^{-1}	M_n/g mol^{-1}	% comp
SP-38	27 500	25 000	7

Fig. 3 DOSY spectra recorded in deuterated acetonitrile yield diffusion coefficients for both the linear polymer (**SP-38-PEGMEMA**) and the Fe^{II}-SCNP generated after irradiation and addition of Fe(BF$_4$)$_2$. The protons used to determine diffusion coefficients are highlighted by coloured spheres that match the corresponding resonance on the ^{1}H NMR spectrum (top). Protons associated with the PMMA backbone were also used, labelled as backbone in the ^{1}H NMR spectrum. The mean value of the diffusion coefficients calculated for the resonances− highlighted in grey − associated with both **SP-38-PEGMEMA** and the **Fe^{II}-SCNP** are represented by a dashed line. The mean diffusion coefficients are used to calculate approximate hydrodynamic diameters. The D_H decreases after irradiation and addition of Fe(BF$_4$)$_2$, indicating that intramolecular folding is occurring leading to an SCNP (for the primary DOSY data of both the Fe^{II}-SCNP and **SP-38-PEGMEMA** refer to ESI section 6†).

polymer **SP-38-PEGMEMA** was exposed to Fe(BF$_4$)$_2$ in the absence of 365 nm light irradiation monitored by SEC. No compaction was observed after 24 h as indicated by the com-

parison of the M_p values before and after introduction of Fe(BF$_4$)$_2$. A small shift to lower apparent molecular weight and narrower *Đ* is observed after 24 h when comparing the corresponding M_n values. PEG is known to form complexes with metal species in a process similar to crown ether complexation.[26–28] The slight shift to a lower apparent molecular weight and narrower *Đ* may be attributed to metal encapsulation by the PEG side chains of the **SP-38-PEGMEMA** polymer. As Fe(BF$_4$)$_2$ induced the largest compaction in the photoinduced folding experiments, further controls with Cu(BF$_4$)$_2$ and Co(BF$_4$)$_2$ were deemed unnecessary. In addition, small molecule ^{1}H NMR studies with the spiropyran monomer, **SP-MMA** were also conducted using 1 min of irradiation and 0.5 equivalents of metal (0.00296 mmol). The photoinduced formation of merocyanine-metal complexes with Fe^{II}, Cu^{II} and Co^{II} was confirmed and the percent composition of Fe^{II} merocyanine was calculated as 17% and 13% for both Cu^{II} and Co^{II} (refer to ESI section 4.1† for the ^{1}H NMR spectra and the procedure). In addition to **SP-38-PEGMEMA**, SCNP formation was attempted on a larger polymer **SP-36-PEGMEMA** (M_n = 40 000 g mol^{-1}; M_p = 45 000 g mol^{-1}) with a similar degree of spiropyran functionalisation (36 mol%) using Co^{II}, Zn^{II} and Ni^{II} (Fig. 4). SCNPs were formed with Co^{II} as evidenced by an approximately 20% reduction in apparent molecular weight. Zn^{II} and Ni^{II} both resulted in a negligible reduction in molecular weight, suggesting that no SCNP formation occurs. Based on these findings, folding was attempted on the polymer **SP-15-PEGMEMA** using Co^{II} and Fe^{II}, similar in size to **SP-38-PEGMEMA**, containing only half the amount of spiropyran units (for SEC traces of **SP-15-PEGMEMA** refer to ESI Fig. S5 and S6†). A less pronounced compaction was observed with Fe^{II}, while no compaction was observed with Co^{II}, suggesting that folding is highly dependent on the number of spiropyran units within the polymer chain.[7] Indeed, graphing the degree of compaction (based on changes in M_p) *vs.* the number of spiropyran units per chain reveals a
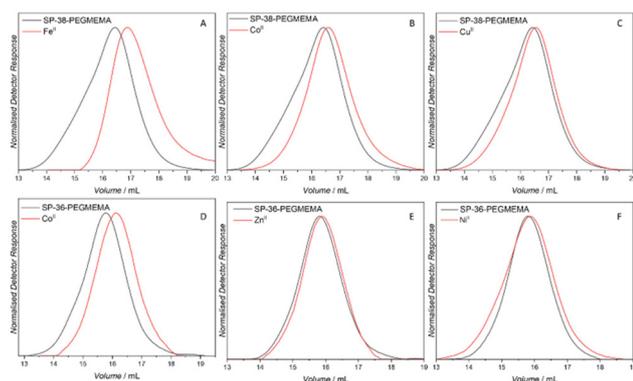
Fig. 4 SEC chromatograms of the photo-induced folding **SP-38/36-PEGMEMA** with late transition metals. (A) **SP-38-PEGEMEMA**-Fe[II], (B) **SP-38-PEGEMEMA**-Co[II], (C) **SP-38-PEGEMEMA**-Cu[II], (D) **SP-36-PEGEMEMA**-Co[II], (E) **SP-36-PEGEMEMA**-Zn[II], (F) **SP-36-PEGEMEMA**-Ni[II]. All chromatograms were recorded in THF as eluent.

Fig. 5 UV-Vis absorption spectra of the linear polymer **SP-36-PEGMEMA** (0.5 g L^{-1}) prior to (SP) and after 365 nm irradiation (MC) as well as of the Fe[II] (red), Co[II] (green) and Cu[II] (yellow) SCNPs generated from **SP-38-PEGMEMA** (0.5 g L^{-1}).

linear correlation for Co[II] and Fe[II] ions, for which we saw the largest compactions (refer to Fig. S23†).

Merocyanine–metal coordination has been shown to occur with a wide variety of metals, displaying a high affinity towards late transition metals.[29] A large number of spiropyran/merocyanine systems rely on the complexation of Cu[II] or Co[II] ions resulting in distinct morphological changes, specifically in polymeric systems, arising from merocyanine complexation.[30–35] In addition, spiropyrans have also been shown to display a high affinity for Fe[II] ions leading to distinct colorimetric responses and selectivity.[36–38] Ions such as Zn[II] or Ni[II] – while known to generate complexes with merocyanine – are less abundant particularly in polymeric systems.[18,39,40] In specific studies examining merocyanine/transition metal complexation, Zn[II] and Ni[II] are often reported as having reduced binding affinity to the open merocyanine. In the current contribution, both Cu[II] and Zn[II] resulted in small compactions compared to that of Fe[II] or Co[II], despite copper being reported to possess a binding affinity that is higher than Co[II] and comparable to Fe[II] in PMMA based polymer systems.[36,41] Compaction may be rationalized by the specific coordination polyhedra of each merocyanine–metal complex. Here, differing geometries (*cis/trans*) with the coordination of a larger or smaller number of polymer/merocyanine ligands to the metal centre may lead to a larger or smaller compaction respectively, analogous to a variation in the number of possible crosslinks in conventional SCNPs.[42] Differences in the composition of the ligand sphere may occur due to steric strain of the polymer backbone as well as different binding energies of the merocyanine ligand to the corresponding metal ion.

The distinct absorption band attributed to the merocyanine (MC) isomer is clearly visible with a λ_{max} of 552 nm in the corresponding UV-Vis spectra after irradiation with a 365 nm LED (refer to Fig. 2A).[19] A blue shift of the absorption maximum is commonly utilised to monitor the complexation of metals to the merocyanine form.[43] Consequently, the UV-Vis
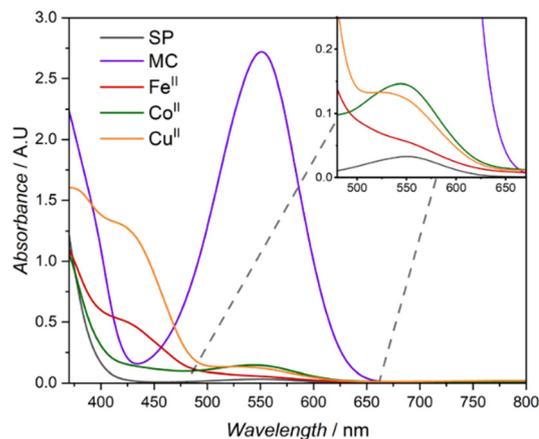
absorption spectra of the different metal containing SCNPs (Fe[II], Co[II] and Cu[II]) reveal distinct absorption profiles similar to metal specific polymeric merocyanine complexes reported in literature. The introduction of Fe[II] and Cu[II] ions resulted in similar absorption spectra with broad absorption profiles expanding into the low visible range (Fig. 5). Spectra of both metals contain two noticeable shoulders, for Fe[II] these are observed at close to 434 and 526 nm and for Cu[II] close to 430 and 535 nm. The two shoulders – approximately 430 and 530 nm – observed in both SCNPs formed from Cu[II] and Fe[II] have been attributed to the presence of complexes arising from the *cis* and *trans* isomer of the merocyanine respectively.[36] In a study by Fries *et al.*, similar absorption profiles for methyl methacrylate based thin film polymers were reported; for Fe[II] the shoulders were observed λ_{max} 520 and 437 nm and for Cu[II] at λ_{max} 520 and 410 nm.[36] Similarly, Byrne *et al.* reported a spiropyran end capped methacrylate polymer capable of complexation with copper leading to the distinct two shoulder profile, with shoulders at 434 and 510 nm.[44] Both studies suggest different complexation processes for the coordination of metals to the merocyanine phenolate and carbonyl of polymeric ester side chains or from the formation of merocyanine metal complexes. In the case of the SCNPs explored in the current study, both binding mechanisms can be envisaged to induce intramolecular crosslinking. Addition of Co[II] results in an absorption spectrum with a profile retaining similarities to un-complexed merocyanine (MC), lacking an absorption band in the low visible region (close to 400 nm) seen in the complexation of Cu[II] and Fe[II]. A distinct absorption band in the mid-visible region is retained with a blue shift to 543 nm compared to 552 nm for the merocyanine maximum absorption. The aforementioned blue-shift is reported in literature for polymeric spiropyran Co[II] complexation, however the absorption is typically blue shifted close to 520 nm.[35]

Conclusions

We introduce a light-driven methodology to compact single polymer chains into single chain nanoparticles (SCNPs) using a polymer system featuring photoreactive spiropyran units in its backbone in different percentages. We find that the degree of single chain compaction is dependent on the specific divalent metal species complexed with the polymer-bound merocyanine. Fe^{II} induced the largest compactions, while smaller compactions are observed when complexing Co^{II}, Cu^{II}, Zn^{II} and Ni^{II}. We attribute this diversity in compaction efficiencies to polymer specific coordination geometries arising from the confinement of merocyanines in the polymer backbone as well as varying ligand–metal bond energies. In addition, the larger the amount of spiropyran units in the polymer backbone, the more pronounced the compaction. Furthermore, increasing the size of the precursor polymer also appears to result in a more significant compaction. Distinct metal specific UV-Vis spectra after compaction *via* spiropyran complexation were used to confirm the incorporation of metals into the structure of the SCNPs. The current findings represent a method of intramolecularly folding a linear polymer into several metal-containing SCNPs using a singular ligand driven by a mild photochemical stimulus.

Conflicts of interest

The authors declare no conflicts of interest.

Acknowledgements

References

1 R. Zeng, L. Chen and Q. Yan, *Angew. Chem., Int. Ed.*, 2020, **59**, 18418–18422.

2 N. D. Knöfel, H. Rothfuss, P. Tzvetkova, B. Kulendran, C. Barner-Kowollik and P. W. Roesky, *Chem. Sci.*, 2020, **11**, 10331–10336.

3 M. Artar, E. R. J. Souren, T. Terashima, E. W. Meijer and A. R. A. Palmans, *ACS Macro Lett.*, 2015, **4**, 1099–1103.

4 A. Levy, R. Feinstein and C. E. Diesendruck, *J. Am. Chem. Soc.*, 2019, **141**, 7256–7260.

5 A. M. Hanlon, C. K. Lyon and E. B. Berda, *Macromolecules*, 2016, **49**, 2–14.

6 H. Frisch, J. P. Menzel, F. R. Bloesser, D. E. Marschner, K. Mundsinger and C. Barner-Kowollik, *J. Am. Chem. Soc.*, 2018, **140**, 9551–9557.

7 J. Engelke, B. T. Tuten, R. Schweins, H. Komber, L. Barner, L. Plüschke, C. Barner-Kowollik and A. Lederer, *Polym. Chem.*, 2020, **11**, 6559–6578.

8 K. Mundsinger, B. T. Tuten, L. Wang, K. Neubauer, C. Kropf, M. L. O'Mara and C. Barner-Kowollik, *Angew. Chem., Int. Ed.*, 2023, **62**, e202302995.

9 J. Chen, K. Li, S. E. Bonson and S. C. Zimmerman, *J. Am. Chem. Soc.*, 2020, **142**, 13966–13973.

10 A. Sathyan, S. Croke, A. M. Pérez-López, B. F. M. de Waal, A. Unciti-Broceta and A. R. A. Palmans, *Mol. Syst. Des. Eng.*, 2022, **7**, 1736–1748.

11 E. Verde-Sesto, A. Arbe, A. J. Moreno, D. Cangialosi, A. Alegría, J. Colmenero and J. A. Pomposo, *Mater. Horiz.*, 2020, **7**, 2292–2313.

12 H. Rothfuss, N. D. Knöfel, P. W. Roesky and C. Barner-Kowollik, *J. Am. Chem. Soc.*, 2018, **140**, 5875–5881.

13 A. Sathyan, L. Deng, T. Loman and A. R. A. Palmans, *Catal. Today*, 2023, **418**, 114116.

14 I. Asenjo-Sanz, T. Claros, E. González, J. Pinacho-Olaciregui, E. Verde-Sesto and J. A. Pomposo, *Mater. Lett.*, 2021, **304**, 130622.

15 M. A. Reith, S. Kardas, C. Mertens, M. Fossépré, M. Surin, J. Steinkoenig and F. E. Du Prez, *Polym. Chem.*, 2021, **12**, 4924–4933.

16 M. A. Sanders, S. S. Chittari, N. Sherman, J. R. Foley and A. S. Knight, *J. Am. Chem. Soc.*, 2023, **145**, 9686–9692.

17 L. Kortekaas and W. R. Browne, *Chem. Soc. Rev.*, 2019, **48**, 3406–3424.

18 T. J. Feuerstein, R. Müller, C. Barner-Kowollik and P. W. Roesky, *Inorg. Chem.*, 2019, **58**, 15479–15486.

19 R. Klajn, *Chem. Soc. Rev.*, 2014, **43**, 148–184.

20 Y. Zhang, M. Cao, B. Yuan, T. Guo and W. Zhang, *Polym. Chem.*, 2017, **8**, 7325–7332.

21 Y. Min, R. Zhang, X. Dong, L. Zhang, D. Qi, Z. Hua and T. Chen, *Polym. Chem.*, 2023, **14**, 888–897.

22 L. Si, Y. Zhang, Y. Yin and C. Wang, *Prog. Org. Coat.*, 2021, **151**, 106080.

23 J. Piard, *J. Chem. Educ.*, 2014, **91**, 2105–2111.

24 K. Kinashi, Y. Harada and Y. Ueda, *Thin Solid Films*, 2008, **516**, 2532–2536.

25 E. Blasco, B. T. Tuten, H. Frisch, A. Lederer and C. Barner-Kowollik, *Polym. Chem.*, 2017, **8**, 5845–5851.

26 M. Patel, H. J. Lee, S. Son, H. Kim, J. Kim and B. Jeong, *Biomacromolecules*, 2020, **21**, 143–151.

27 M. M. Hoffmann, *Curr. Opin. Colloid Interface Sci.*, 2022, **57**, 101537.

28 J. F. Rabek, J. Lucki, B. J. Qu and W. F. Shi, *Macromolecules*, 1991, **24**, 836–843.

29 A. Perry and C. J. Kousseff, *Beilstein J. Org. Chem.*, 2017, **13**, 1542–1550.

30 M. Natali, C. Aakeröy, J. Desper and S. Giordani, *Dalton Trans.*, 2010, **39**, 8269–8277.

31 N. Shao, Y. Zhang, S. Cheung, R. Yang, W. Chan, T. Mo, K. Li and F. Liu, *Anal. Chem.*, 2005, **77**, 7294–7303.

32 E. S. Epstein, L. Martinetti, R. H. Kollarigowda, O. Carey-De La Torre, J. S. Moore, R. H. Ewoldt and P. V. Braun, *J. Am. Chem. Soc.*, 2019, **141**, 3597–3604.

33 N. Ye, Y. Pei, Q. Han and L. Y. Jin, *Soft Matter*, 2023, **19**, 1540–1548.

34 D. Liu, W. Chen, K. Sun, K. Deng, W. Zhang, Z. Wang and X. Jiang, *Angew. Chem., Int. Ed.*, 2011, **50**, 4103–4107.

35 H. Cui, H. Liu, S. Chen and R. Wang, *Dyes Pigm.*, 2015, **115**, 50–57.

36 K. H. Fries, J. D. Driskell, S. Samanta and J. Locklin, *Anal. Chem.*, 2010, **82**, 3306–3314.

37 K. H. Fries, J. D. Driskell, G. R. Sheppard and J. Locklin, *Langmuir*, 2011, **27**, 12253–12260.

38 Z. Yang, F. Wang and H. Liu, *J. Polym. Res.*, 2019, **26**, 89.

39 A. Dunne, C. Delaney, A. McKeon, P. Nesterenko, B. Paull, F. Benito-Lopez, D. Diamond and L. Florea, *Sensors*, 2018, **18**, 1083.

40 E. D. Canto, M. Natali, D. Movia and S. Giordani, *Phys. Chem. Chem. Phys.*, 2012, **14**, 6034–6043.

41 X. Xiao, C. Zhang, L. Chen and L. Liao, *React. Funct. Polym.*, 2021, **160**, 104824.

42 H. Rothfuss, N. D. Knöfel, P. Tzvetkova, N. C. Michenfelder, S. Baraban, A.-N. Unterreiner, P. W. Roesky and C. Barner-Kowollik, *Chem. – Eur. J.*, 2018, **24**, 17475–17486.

43 M. Huang, J. Zhou, X. Zheng, Y. Zhang, S. Xu and Z. Li, *Inorg. Chem. Commun.*, 2020, **117**, 107968.

44 R. Byrne, C. Ventura, F. Benito Lopez, A. Walther, A. Heise and D. Diamond, *Biosens. Bioelectron.*, 2010, **26**, 1392–1398.